

Chair of Optoelectronics  
Institute of Computer Engineering  
Universität Heidelberg

# Annual Report

## 2015 - 2016

# CONTENTS

Staff .....	II
Foreword .....	III
Research Projects .....	IV
Publications 2015 - 2016.....	9
Imprint.....	10

# STAFF



**Prof. Dr.  
Karl-Heinz Brenner**  
Head of the Chair



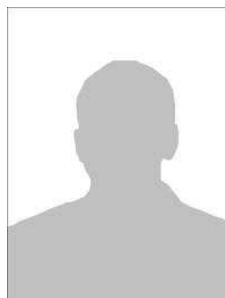
**Sabine Volk**  
Secretary



**Wolfgang Stumpfs**  
Technical Assistant



**Tim Stenau**  
PhD-Student



**Soheil Mehrabkhani**  
PhD-Student  
(no picture available)



**André Junker**  
PhD-Student



## FOREWORD

Dear reader,

This annual report describes the research activities of the chair of optoelectronics for the years 2015-2016. The contribution on page 2 illustrates that scalar light propagation algorithms in the spatial domain, although having been used for many years and for many applications, have a severe imperfection that can be solved. A significant amount of work has been done in the field of rigorous simulations. We developed a criterion for the correctness, which does not rely on a comparison with other methods. In the first article, we employ conservation laws as a criterion for accuracy. In the contributions on page 6-7, we explored extensions to the traditional methods, such as allowing the incident and transmitted regions to be structured or allowing the incident illumination to be structured. On page 5, we extended the RCWA to structures beyond simple rectangles and the contribution on page 8 tries to get rid of physical dimensions and natural constants by separating the theoretical description into a physical and a computational part. Another activity concerns applications and tests of the diffractive overlapping lenses, reported before in the previous annual report. We developed a criterion for comparing diffractive lenses to refractive ones on page 3 and demonstrated the application to microscopy on page 4.

We hope that many of the topics in this report will find your interest.

Karl-Heinz Brenner  
*Head of the chair*

# RESEARCH PROJECTS

<b>M. Auer, K.-H. Brenner</b>	
<i>Verification of near-field calculations by conservation laws .....</i>	<i>1</i>
<b>S. Mehrabkhani, K.-H. Brenner</b>	
<i>Modification of spatial domain algorithms for apertureless light propagation.....</i>	<i>2</i>
<b>T. Stenau, K.-H. Brenner</b>	
<i>Analysis of the focusing efficiency of diffractive lenses with overlapping apertures with respect to typical fabrications constrains .....</i>	<i>3</i>
<b>T. Stenau, K.-H. Brenner</b>	
<i>Imaging with a parallel scanning microscope using diffractive lenses with overlapping apertures.....</i>	<i>4</i>
<b>K.-H. Brenner</b>	
<i>Elementary building blocks for a more flexible layer definition in the RCWA.....</i>	<i>5</i>
<b>A. Junker, K.-H. Brenner</b>	
<i>Structuring the incident and transmitted regions in rigorous coupled-wave analysis .....</i>	<i>6</i>
<b>A. Junker, K.-H. Brenner</b>	
<i>Simulation and analysis of SNOM-measurements using rigorous coupled-wave analysis .....</i>	<i>7</i>
<b>K.-H. Brenner</b>	
<i>Normalized electromagnetic fields .....</i>	<i>8</i>

# Verification of near-field calculations by conservation laws

M. Auer, K.-H. Brenner

There are several methods to solve Maxwell's equations numerically exact. Although these algorithms describe an exact theory, any deviations from the accurate solution may still occur algorithmically, due to finite mesh size or due to mode truncation. An experimental verification of the near fields is usually very difficult.

The standard verification in the rigorous coupled wave analysis (RCWA) uses the sum of transmission and reflection coefficients which should be one for the case of a non-absorbing structure. In case of materials with an extinction coefficient, this definition is used for calculating the absorption in the structure, thus eliminating the possibility for verification. Therefore we propose to use conservation laws for verification.

The Gauss Law relates a surface integral to the volume integral over the divergence of an analytic field:

$$\oiint \vec{F} \cdot d\vec{A} = \iiint \text{div}(\vec{F}) dV \quad (1)$$

For the surface integral (left), we can identify  $\vec{F}$  with the electric field, calculated from the transmission and reflection coefficients. For the volume integral (right), the divergence can be related to the local absorption according to Poynting's theorem [1]. Thus we have a relation between the near fields and the far fields, which can be tested.

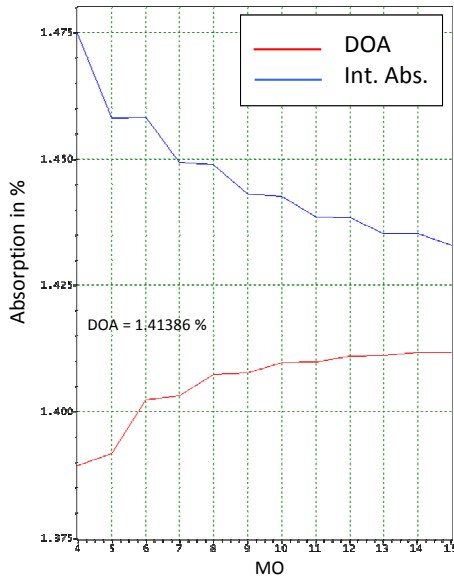


**Fig 1:** Comparison of absorption depending on mode count calculated from far fields (DOA) to absorption calculated from near fields (Int.Abs.) for the case of applying Li's rule as is usually done in the standard RCWA.

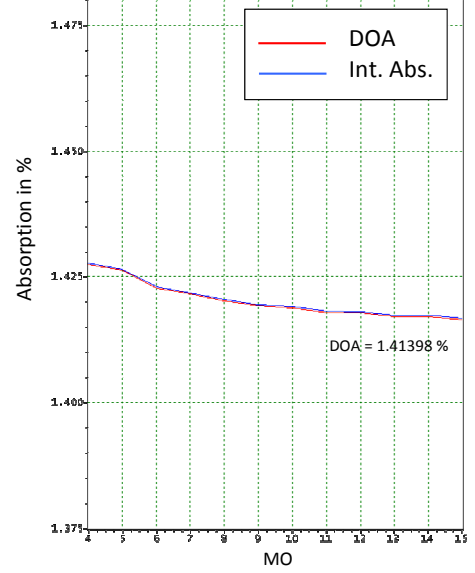


**Fig. 2:** Comparison of absorption depending on mode count calculated from far fields (DOA) to absorption calculated from near fields (Int. Abs.) for a new method described in [2].

The comparisons in fig. 1 and fig. 2 indicate that the application of Li's rule introduces an inconsistency between near and far fields, which is observable by a discrepancy in the absorption values. This discrepancy can be removed by an alternative way of calculating the near fields in a structure which was first described in [1] and later was extended to structured illumination [2]. The results in this publication clearly indicate, that the deviations between near and far field absorption range between 1 and 4 percent for different known calculation methods but assume values of close to zero for this new method.

## References:

- [1] K.-H. Brenner, "Aspects for calculating local absorption with the rigorous couple-waved method", Optics Express, Vol. 18, Iss. 10, pp. 10369-10376, (2010)
- [2] M. Auer, K.-H. Brenner, "Localized input fields in rigorous coupled-wave analysis", J. Opt. Soc. Am. A, Vol. 31, No. 11, (2014)

# Modification of spatial domain algorithms for apertureless light propagation

S. Mehrabkhani, K.-H. Brenner

Light propagation algorithms in the spatial domain hold an implicit assumption that the calculation region represents a virtual aperture, i.e., the amplitude outside of the calculation region is zero. With typically bright objects on a dark background, this assumption is valid. With dark objects on a bright background, however, the assumption is violated and the calculation result is dominated by diffraction effects at a virtual aperture. This problem is particularly severe for pure phase elements, because the amplitude outside the calculation region is constant one.

The existing algorithms for scalar light propagation, can be divided into two types, spatial domain algorithms and frequency domain algorithms. For the frequency domain algorithms, like Angular spectrum method or the Fresnel approximation, the input is assumed to be periodic and the algorithm is only valid in the near field, as long as there is no spill-over from neighbouring periods. On the other hand, spatial domain algorithms such as the Rayleigh-Sommerfeld integral or the Engelberg-Ruschin-approximation [1] are only valid in the mid to far field and do not show this behaviour. For these algorithms, however, another problem occurs. If the field outside the calculation region is not zero, significant aperture diffraction is observable at the edges of the calculation region as illustrated in Fig 1.

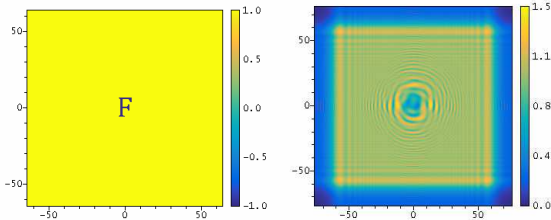


**Fig. 1:** Left: Phase element (real part) with corresponding diffraction amplitude (right). The result is disturbed by unphysical edge diffraction.

To remove the virtual aperture diffraction problem, we proposed the following correction approach [2]: Consider an input field  $u(\vec{r}_\perp, 0)$  defined in the two-dimensional space  $\mathbb{R}^2$  which can have variable values  $u_\Omega(\vec{r}_\perp, 0)$  over the calculation domain  $\Omega$  and a constant value  $u_0$  outside of the domain

$$u(\vec{r}_\perp, 0) = \begin{cases} u_0 & \vec{r}_\perp \notin \Omega \\ u_\Omega(\vec{r}_\perp, 0) & \vec{r}_\perp \in \Omega \end{cases} \quad (1)$$

Without loss of generality we can equivalently rewrite  $u$  as an addition of two new fields as follows:

$$u_1(\vec{r}_\perp, 0) = u_0 \quad \vec{r}_\perp \in \mathbb{R}^2$$

$$u_2(\vec{r}_\perp, 0) = \begin{cases} u_\Omega(\vec{r}_\perp, 0) - u_0 & \vec{r}_\perp \in \Omega \\ 0 & \vec{r}_\perp \notin \Omega \end{cases} \quad (2)$$

This very simple reformulation of the input field has a valuable advantage. The first field  $u_1 = u_0$  is a uniform field over the whole space  $\mathbb{R}^2$  and the second one  $u_2 = u_\Omega(\vec{r}_\perp, 0) - u_0$  has only nonzero values over the domain  $\Omega$ . Now because of the uniformity of the field  $u_1(\vec{r}_\perp, 0) = u_0$  the corresponding propagated field at distance  $z$  is simply  $u_1(\vec{r}_\perp, z) = u_0 e^{ikz}$ . The second part  $u_2(\vec{r}_\perp, z)$  vanishes outside of the domain  $\Omega$  and can be numerically computed with any spatial domain algorithm.

$$u_1(\vec{r}_\perp, z) = P_A(u_0) \quad \vec{r}_\perp \in \mathbb{R}^2$$

$$u_2(\vec{r}_\perp, z) = P_N(u_\Omega(\vec{r}_\perp, 0) - u_0) \quad \vec{r}_\perp \in \Omega \quad (3)$$

Here,  $P_A$  stands for an analytic propagation and  $P_N$  for a numerical propagation with possible approximation errors. Because the input field is an exact sum of the two components, but the  $u_0$ -part is treated analytically and the other part numerically, the approximation errors in the term  $u_\Omega - u_0$  cancel each other and thus the diffraction at the virtual aperture is automatically removed for all types of numerical propagators. This correction is essential for the proper treatment of lensless holography, an established method using phase retrieval in microscopy to obtain holographic information from far field measurements.

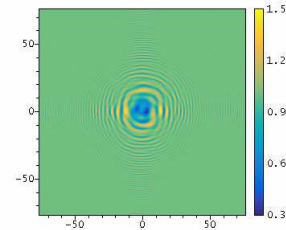


**Fig. 2:** Diffraction amplitude of the phase element of fig. 1, applying the corrections described.

## References:

- [1] Y.M. Engelberg, S. Ruschin, "Fast method for physical optics propagation of high numerical aperture beams", J. Opt. Soc. Am., Vol. **21**, No. 11, pp. 2135-2145, (2004)
- [2] K.-H. Brenner, S. Mehrabkhani "Modification of spatial domain algorithms for apertureless light propagation", Appl. Opt., Vol. **56**, No. 1, A8 – A12, (2017)

# Analysis of the focusing efficiency of diffractive lenses with overlapping apertures with respect to typical fabrications constrains

T. Stenau, K.-H. Brenner

Diffractive lenses with overlapping apertures enable a dense spot-wise illumination with high aperture foci, which is not achievable with traditional refractive lens arrays. Particularly the numerical aperture (NA) of a diffractive lens with overlapping apertures is a free design parameter and independent of the focal length and the focal pitch of the lens array. The question arises how these lenses perform in terms of focusing efficiency [1]. To evaluate this quantity, a ratio similar to the Strehl ratio is used,

$$S_{\text{mod}} = \frac{I(0, f)}{I_{\text{ideal}}(0, f)} \frac{P_{\text{ideal}}}{P} \quad (1)$$

where the peak intensity  $I(0, f)$  produced by a lens array with overlapping apertures is compared to the focal intensity  $I_{\text{ideal}}(0, f)$  of the “perfect wave” [2] with an aperture determined by the NA. The power of the waves is used for normalization. Due to the overlap, the incident power per period is used for  $P$ , whereas  $P_{\text{ideal}}$  is the power falling into the full aperture. This definition allows to assess the influences of overlap as well as the influences due to typical fabrication constraints and errors.

In Fig. 1, the effect of phase quantization is plotted for lens arrays with fixed pitch and focal length but different numerical apertures.

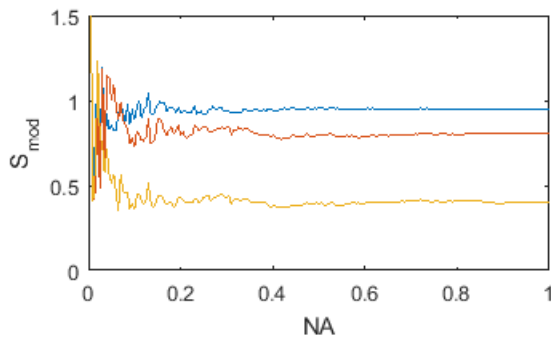


**Fig. 1:** Relative light concentration efficiency for lens arrays with continuous amplitude and 2 (orange), 4 (red) and 8 (blue) discrete phase levels.

For high numerical apertures, the phase quantization results in a simple multiplicative loss. The amount agrees well with the upper diffraction efficiency bound given in the literature [3].

In Fig. 2, the effect of sole amplitude leveling and amplitude leveling combined with phase binarization is shown. For comparison, the relative light concentration efficiency for arrays with continuous amplitude and with or without phase binarization is shown.

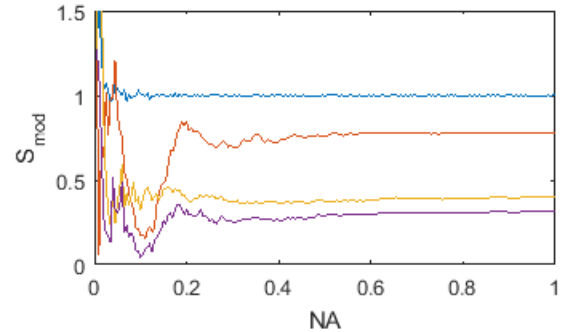


**Fig. 2:** Relative light concentration efficiency for elements with continuous amplitude and phase (blue), leveled amplitude and continuous phase (red), continuous amplitude and binarized phase (orange) and leveled amplitude and binarized phase (violet).

Again, for high numerical apertures, the amplitude leveling results in a multiplicative loss. The effects from phase quantization and amplitude leveling seem to be independent. The loss factor in the case of a leveled amplitude and binarized phase is the product of the loss factors of each individual effect. For lower numerical apertures, a severe deviation from a constant loss factor is found. The reason for this is shown in Fig. 3. For low numerical apertures the amplitude leveling results in a modulation of the focal profile.

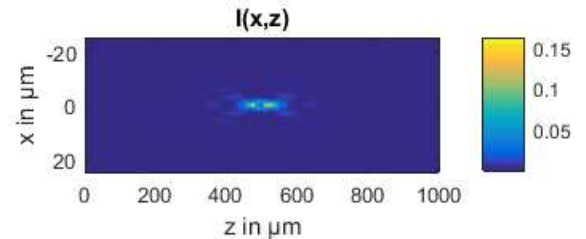


**Fig. 3:** Focal profile of an amplitude leveled diffractive lens with overlapping apertures with focal length 500 $\mu\text{m}$ , focal pitch 44 $\mu\text{m}$  and NA 0.1 for the wavelength 0.5  $\mu\text{m}$ .

Due to this, the Strehl criterion is not suited to assess the quality of the foci. For higher numerical apertures the focal profile remains smooth even when post-processing is applied, therefore the Strehl criteria stays valid.

## References:

- [1] T. Stenau, K.-H. Brenner, “Light concentration efficiency of diffractive lenses with overlapping apertures”, DGaO-Proceedings, 117<sup>th</sup> Annual Meeting, Hannover, (2016)
- [2] J. J. Stamnes, “Focusing of a perfect wave and the Airy pattern formula I”, *Opt. Commun.*, Vol. **37**, No.5, pp. 311-314, (1981)
- [3] W. H. Welch, J. E. Morris, M. R. Feldman, “Iterative discrete on-axis encoding of radially symmetric computer-generated holograms”, *J. Opt. Soc. Am. A*, Vol. **10**, No. 8, pp. 1729-1738, (1993)

# Imaging with a parallel scanning microscope using diffractive lenses with overlapping apertures

T. Stenau, K.-H. Brenner

Scanning microscopy in principle solves the typical trade off between resolution and field of view at the cost of large scanning times. Therefore, parallelization is beneficial. Here, the setup and experimental images of a parallel scanning microscope which uses diffractive lenses with overlapping aperture are presented [1]. Diffractive lenses with overlapping apertures eliminate the strict relations between focal length, lens diameter and pitch, existing with refractive micro-lens arrays and therefore a high resolution, a large field of view, a large working distance and faster scan rates become feasible at the same time.

The experimental realisation of our parallel scanning microscope is shown in figure 1.



Fig. 1: Experimental realisation of the scanning microscope.

An expanded NG:YAG-laser ( $\lambda = 0.532 \mu\text{m}$ ) creates a plane wave illumination for the diffractive element, resulting in a focalspot-array intensity on the sample. The focal positions are controlled by shifting the element with a xyz-piezo stage. Due to the large focal length, there is sufficient working distance to place the specimen in a sample holder beneath the element. The illuminated sample is observed from below with an imaging optics. The element periodicity of  $44 \mu\text{m}$  secures, that there is no crosstalk between adjacent spots.

The parallel imaging process is described with standard confocal scanning microscopy theory, but the physical confocal aperture is replaced by a virtual, digital aperture. The image intensity is given by

$$I = |(h_{illum} h_{obs}) \otimes u_{obj}|^2 \approx |(h_{illum}) \otimes u_{obj}|^2, \quad (1)$$

where  $h_{illum}$  and  $h_{obj}$  are the point spread functions of the illumination and imaging optics, which are convolved with the complex amplitude of the examined object  $u_{obj}$ . The approximation is valid for

observation optics with low numerical aperture which enables a large field of view.  $h_{illum}$  is determined by the illumination spot NA of 0.48.

In figure 2, reconstructions of a resolution test chart are shown. Each period of  $44 \mu\text{m}$  is sampled with 240 steps. The maximal resolved penta bar with non vanishing contrast is 1100 lp/mm, this corresponds to a minimal resolved feature size of 450 nm.

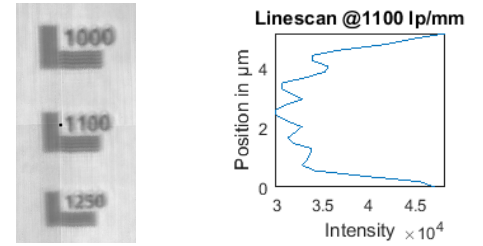


Fig. 2: Reconstruction of a resolution chart. The line scan shows that a maximum of 1100 lp/mm can be resolved.

To demonstrate the large field of view of this setup a reconstructed image of approx.  $900 \mu\text{m} \times 1200 \mu\text{m}$  with 550 nm pixel size is shown in figure 3.



Fig. 3: Reconstructed image with a field of view of approx.  $900 \mu\text{m} \times 1200 \mu\text{m}$ .

To sum it up, the imaging with a parallel scanning microscope using diffractive lenses with overlapping apertures with 2 mm working distance and a  $900 \mu\text{m} \times 1200 \mu\text{m}$  field of view, which is capable of resolving features of about 450 nm was experimentally demonstrated.

## Reference:

[1] T. Stenau, K.-H. Brenner, "Diffractive Lenses with Overlapping Aperture - A New Tool in Scanning Microscopy", Imaging Systems and Applications, Optical Society of America, IT1F-1, 25.-28.7.16, Heidelberg, (2016)

# Elementary building blocks for a more flexible layer definition in the RCWA

*K.-H. Brenner*

All the existing RCWA implementations use the rectangular function as an elementary building block for defining the permittivity distribution in a layer. We denote this as the constant segment (CS). For gratings, this approach is fully appropriate. For graded structures such as sinusoidal gratings, this approach is not satisfactory, since the rectangular steps have to be adjusted very fine, in order to avoid approximation errors.

Here we suggest two new building blocks, which may be used to cover a wide range of permittivity distributions. The first is the linear segment (LS) as shown in fig. 1.

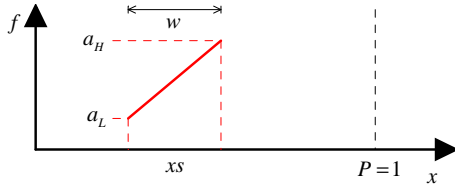


**Fig. 1:** Definition of linear segment.

It is characterized by a center value  $x_s$ , a width  $w$  and upper and lower values  $a_H$  and  $a_L$ . With this building block, imperfect transitions can be modelled very accurately.

A second building block, we suggested and implemented is the trigonometric segment (TS), as shown in fig. 2. It is characterized by the same quantities as the linear segment.

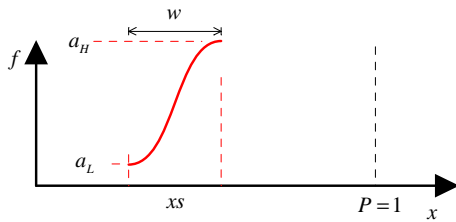


**Fig. 2:** Definition of trigonometric segment.

The trigonometric segment is especially useful for avoiding the Gibbs phenomenon, an oscillatory phenomenon well known and observable for the rectangular segment. By adjusting the transitions smoothly, reliable results can be obtained without going to an extremely high mode count.

For these two additional segments, the mode coefficients can be calculated analytically and due to the linearity of the problem, the result can be simply added. Fig. 3 illustrates the use of the trigonometric segments. The red curve is a 10-mode-reconstruction

of 3 constant segments with widths 0.25, 0.5, 0.25, showing the typical Gibbs phenomenon. The blue curve is a 10-mode-reconstruction of a sequence of CS, TS, CS, TS, CS with the widths (0.185, 0.13, 0.37, 0.13, 0.185). It is clearly visible that this definition of a rectangular structure suffers much less from Gibbs phenomenon.

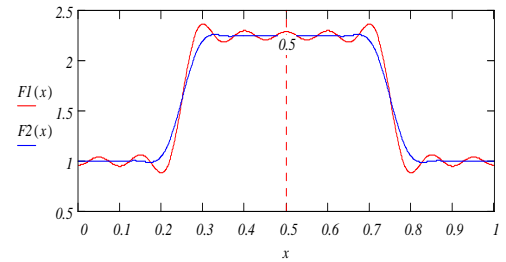


**Fig. 3:** Comparison of reconstructions with 10 modes: Red: three constant segments, blue: 5 segments with 2 TS at the edges of the rectangle. The Gibbs phenomenon can be suppressed efficiently.

In fig 4, we constructed a layer with linear absorbing edges, similar to a PML. This way, the spreading of light into neighboring periods is efficiently suppressed.

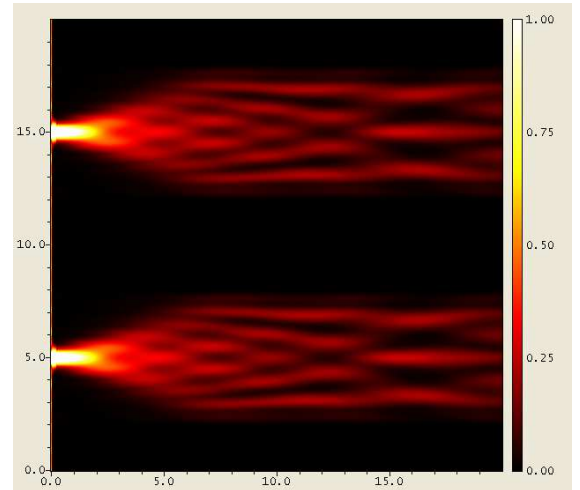


**Fig. 4:** Implementation of a PML by two linear absorbing segments at the edge of the period.

# Structuring the incident and transmitted regions in rigorous coupled-wave analysis

A. Junker, K.-H. Brenner

In the common implementation of the rigorous coupled-wave analysis (RCWA) a periodic grating structure is situated between the incident and transmitted regions, assumed to be homogeneous. Furthermore, a plane wave is assumed to be incident from  $z = -\infty$ . In the following, we extend the RCWA to the treatment of both structured incident and transmitted regions, and structured illumination in the form of a superposition of multiple modes.

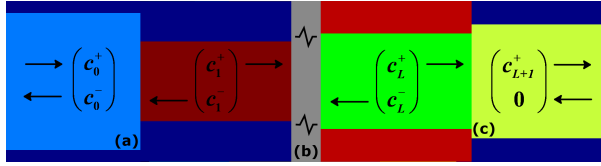


**Fig. 1:** RCWA with both structured incident and transmitted regions and structured illumination.

To this end, an eigenmode decomposition is performed for the incident and transmitted regions the same way it is done for the grating layers [1]. Furthermore, we apply the approach described in [2] in order to achieve a structured illumination. Subsequently, the tangential electric and magnetic field components are matched at the interfaces (see Fig. 1). The incident field's eigenmode coefficients  $\mathbf{c}_0^+$  are given. The reflected and transmitted eigenmode coefficients  $\mathbf{c}_0^-$  and  $\mathbf{c}_{L+1}^+$  are to be computed. The boundary conditions between successive layers are

$$\begin{aligned} \begin{pmatrix} W_0 & W_0 \\ V_0 & -V_0 \end{pmatrix} \begin{pmatrix} \mathbf{c}_0^+ \\ \mathbf{c}_0^- \end{pmatrix} &= \begin{pmatrix} W_1 & W_1 X_1 \\ V_1 & -V_1 X_1 \end{pmatrix} \begin{pmatrix} \mathbf{c}_1^+ \\ \mathbf{c}_1^- \end{pmatrix} \\ \begin{pmatrix} W_{l-1} X_{l-1} & W_{l-1} \\ V_{l-1} X_{l-1} & -V_{l-1} \end{pmatrix} \begin{pmatrix} \mathbf{c}_{l-1}^+ \\ \mathbf{c}_{l-1}^- \end{pmatrix} &= \begin{pmatrix} W_l & W_l X_l \\ V_l & -V_l X_l \end{pmatrix} \begin{pmatrix} \mathbf{c}_l^+ \\ \mathbf{c}_l^- \end{pmatrix} \\ \begin{pmatrix} W_L X_L & W_L \\ V_L X_L & -V_L \end{pmatrix} \begin{pmatrix} \mathbf{c}_L^+ \\ \mathbf{c}_L^- \end{pmatrix} &= \begin{pmatrix} W_{L+1} & W_{L+1} \\ V_{L+1} & -V_{L+1} \end{pmatrix} \begin{pmatrix} \mathbf{c}_{L+1}^+ \\ \mathbf{c}_{L+1}^- \end{pmatrix} \end{aligned} \quad (1)$$

Note that the incident region (index 0) and the transmitted region (index  $L+1$ ) are now structured. The matrices  $W_i$ ,  $V_i$ ,  $X_i$  are defined as in [1]. It is easy to see that this approach is consistent with the common RCWA [3]. To satisfy the boundary conditions would be the next step of calculation. To this end we need to know the propagation direction of all the eigenmodes. As outlined in detail in Ref. [3], the definition of the propagation direction of a *general* eigenmode of a structured layer is not straightforward and must be de-

termined from its Poynting vector

$$\langle \mathbf{S} \rangle(\mathbf{x}) = \frac{1}{2} \text{Re} \left[ \mathbf{E}(\mathbf{x}) \times \mathbf{H}^*(\mathbf{x}) \right].$$

It can be concluded by integrating the Poynting vector's  $z$ -component over one period [3],

$$\begin{aligned} \iint_{P_x P_y} \langle S_z \rangle_N(\mathbf{x}, z) dx dy \\ = \frac{1}{2} e^{2k_0 \text{Re}[q_N]z} \sum_m \text{Re} \left[ w_{x,mN} v_{y,mN}^* - w_{y,mN} v_{x,mN}^* \right] \end{aligned} \quad (2)$$

For several special cases an analytic solution for the Poynting vector exists [3]. The presented algorithm can be applied to several interesting problems that cannot be simulated with the common RCWA. As an example we present evanescent mode coupling between adjacent waveguides (see Fig. 2), where two infinitely long step index fibers are placed in close proximity to each other and the eigenmode of a single waveguide is incident onto the upper fiber. As expected, the power is oscillating perfectly between the waveguides.

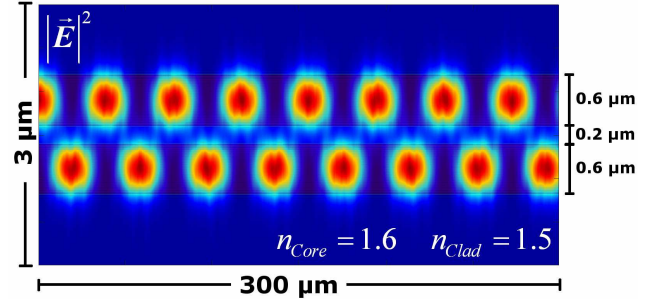


**Fig. 2:** RCWA simulation of evanescent coupling between two waveguides.  $\lambda = 633 \text{ nm}$ , 201 modes.

Further examples and applications of the presented algorithm can be found in Ref. [3].

## References:

- [1] M. G. Moharam and T. K. Gaylord, "Rigorous coupled-wave analysis of planar-grating diffraction", J. Opt. Soc. Am. A, Vol. **71**, No. 7, pp. 811–818, (1981)
- [2] M. Auer, K.-H. Brenner, "Localized input fields in rigorous coupled-wave analysis", J. Opt. Soc. Am. A, Vol. **31**, No. 11, pp. 2395–2393, (2014)
- [3] A. Junker, K.-H. Brenner, "Structuring the incident and transmitted regions in rigorous coupled-wave analysis", 15<sup>th</sup> Workshop on Information Optics (WIO), IEEE, 978-1-5090-2163-5/16, 11.-15 July 2016, Barcelona/Spain, (2016)

# Simulation and analysis of SNOM-measurements using rigorous coupled-wave analysis

A. Junker, K.-H. Brenner

Rigorous Coupled-Wave Analysis (RCWA) is applied to analyze various influences on the resolution of Scanning Near-field Optical Microscopy (SNOM) images. Furthermore, we simulate how the presence of a fiber tip alters the electromagnetic field during a measurement and compare the numerical result to the undisturbed electric field intensity.

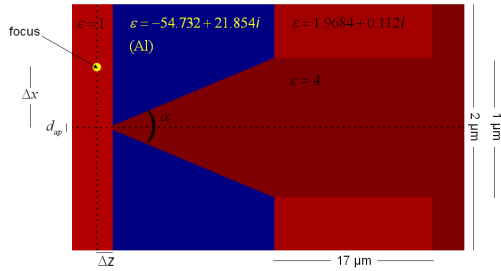


**Fig. 1:** Permittivity distribution of the fiber tip (top).

First, a simulated SNOM-measurement is conducted, where a narrow sub-wavelength spot ( $\sim 25\text{nm}$ ) serves as a sample under test. Fig. 1 illustrates the permittivity distribution of the fiber tip with  $d_{ap}$  (aperture diameter),  $\alpha$  (apex angle),  $\Delta z$  (longitudinal distance sample-aperture) and  $\Delta x$  (lateral offset). The focus is moved laterally across the aperture and a RCWA calculation is conducted at each  $\Delta x$  ( $\lambda = 850\text{nm}$ ,  $P = 2\mu\text{m}$ , 101 modes). We obtain an intensity profile by plotting the amount of power coupled into the fiber core versus  $\Delta x$ . The LIF-RCWA [1] is applied to excite the 81 central modes of the incident field in TM polarization to generate the  $25\text{nm}$  spot.

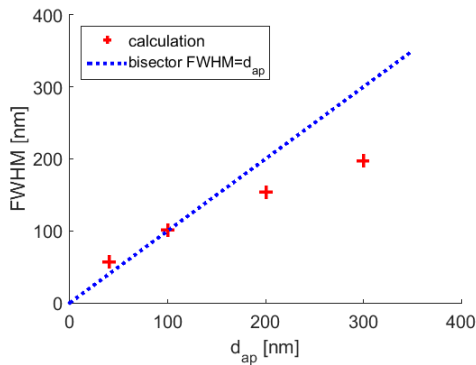


**Fig. 2:** Full width at half maximum (FWHM) of the measured peak versus  $d_{ap}$ .

We investigate the influence of the parameters  $d_{ap}$ ,  $\alpha$ , and  $\Delta z$  on the width of the measured intensity profile. We observe that the width of the recorded peak is approximately proportional to the width of the tip

aperture (see Fig. 2). As expected, the amount of intensity coupled into the fiber core increases for larger aperture diameters. Increasing the apex angle  $\alpha$  does not significantly change the width of the recorded peak, but the amount of intensity coupled into the fiber core grows. Furthermore, we observe that the peak width increases with larger  $\Delta z$  (from  $\sigma = 24\text{nm}$  at  $\Delta z = 30\text{nm}$  to  $\sigma = 143\text{nm}$  at  $\Delta z = 200\text{nm}$ ). The latter observation can be explained by the characteristic exponential decay of evanescent modes.

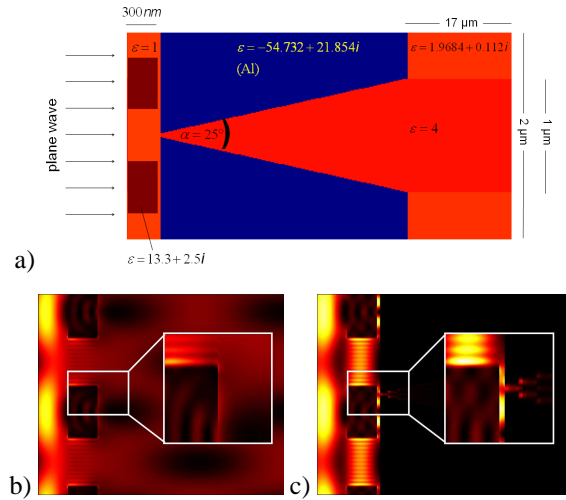


**Fig. 3:** Permittivity distribution of the grating structure and the fiber tip (a). Power density distribution without (b) and with (c) fiber probe inserted.  $d_{ap} = 40\text{nm}$ ,  $\Delta z = 30\text{nm}$ .

In the second step we conduct a simulated SNOM-measurement of a back-illuminated grating structure in order to investigate the influence of the presence of the fiber tip on the measurement. Fig. 2 (a) illustrates the simulated permittivity distribution. In Fig. 2 (b,c) the power density distribution is shown without and with the fiber tip for one particular tip position  $\Delta x$ . It can be seen that the presence of the tip severely disturbs the power density distribution. By scanning this grating structure in  $\Delta x$  we find that the measured width of the refractive index step  $\sigma \approx 43\text{nm} \approx \lambda/20$  is small, but its position is shifted by approximately  $\delta x \approx 82\text{nm}$  with respect to the original step position of the grating [2].

## References:

- [1] M. Auer, K.-H. Brenner, "Localized input fields in rigorous coupled-wave analysis", J. Opt. Soc. Am. A, Vol. **31**, No. 11, pp. 2385-2393, (2014)
- [2] A. Junker, K.-H. Brenner, "Simulation and Analysis of SNOM Measurements using Rigorous Coupled-Wave Analysis", DGAO-Proceedings, 116<sup>th</sup> Annual Meeting in Brno / Czech Republic, (2015)

# Normalized electromagnetic fields

*K.-H. Brenner*

There are many situations in optical design, where rigorous electromagnetic calculations are necessary, because the usual scalar approximations are not sufficient. In this case, the solution of Maxwell's equations must be determined numerically. The quantities in Maxwell's equations are associated with physical dimensions, which shift the number range, depending on whether we work with mW or MW of illumination. Ideally, one would like to consider the incident electric field as dimensionless with a magnitude of one. In the initial stable treatment of the rigorous coupled wave analysis (RCWA) by Moharam [1], independence of dimensions is attempted by defining the electric and magnetic field as

$$\begin{aligned} E_y &= \sum_i S_{y_i}(z) \exp(-jk_{x_i}x) \\ H_x &= -j \left( \frac{\epsilon_0}{\mu_0} \right)^{\frac{1}{2}} \sum_i U_{x_i}(z) \exp(-jk_{x_i}x) \end{aligned} \quad (1)$$

Thus the coefficient  $S$  and  $U$  have the dimension of an electric field. Consequently the coefficient vectors  $\mathbf{c}^+$  and  $\mathbf{c}^-$ , which satisfy the continuity condition

$$\begin{pmatrix} \mathbf{WX} & \mathbf{W} \\ \mathbf{VX} & -\mathbf{V} \end{pmatrix} \begin{pmatrix} \mathbf{c}^+ \\ \mathbf{c}^- \end{pmatrix} = \begin{pmatrix} \mathbf{T} \\ i\mathbf{Y}_H \mathbf{T} \end{pmatrix} \quad (2)$$

also have a physical dimension. But  $\mathbf{T}$  should be a ratio of transmitted to incident E-field. This example tries to motivate that it would be desirable to have a definition which is not dependent on the physical dimensions of the illumination and which can be transformed into a description having the correct physical dimensions.

In our implementation we tried to separate the numerical part from the physical part, by defining

$$\mathbf{E}(\mathbf{r}) = E_0 \mathbf{E}^1(\mathbf{r}) \quad (4)$$

Here,  $E_0$  is the physical part, expressing the electrical field strength in V/m, whereas  $\mathbf{E}^1$  is a dimensionless quantity, used in the numerical calculations. Likewise, we define

$$\mathbf{H}(\mathbf{r}) = \frac{E_0}{Z_0} \mathbf{H}^1(\mathbf{r}) \quad (5)$$

such that  $\mathbf{H}$  is a true magnetic field with dimension A/m and  $\mathbf{H}^1$  is dimensionless. With these definitions, the first two Maxwell equations can be written as

$$\begin{aligned} \vec{\nabla} \times \mathbf{E}^1 &= ik_0 \mu \mathbf{H}^1 \\ \vec{\nabla} \times \mathbf{H}^1 &= -ik_0 \epsilon \mathbf{E}^1 \end{aligned} \quad (6)$$

with  $i$  now being the imaginary unit for physicists. Now  $\mathbf{E}^1$  and  $\mathbf{H}^1$  are only connected by a quantity of dimension  $m$ , which is derived from the sampling distance determined by the gradient at the left side of eq. 6.

The energy density in this definition can be split into a physical and a numerical part:

$$w = \frac{\epsilon_0}{2} E_0^2 \frac{1}{2} \text{Re} \left( \epsilon |\mathbf{E}^1|^2 + \mu |\mathbf{H}^1|^2 \right) \quad (7)$$

indicating that the physical energy density is derived from the computational one by multiplication with a fixed factor. Similarly, the physical Poynting vector is expressed as

$$\mathbf{S} = \frac{E_0^2}{Z_0} \frac{1}{2} \text{Re} \left( \mathbf{E}^1 \times \mathbf{H}^1 \right) \quad (8)$$

allowing the term  $\frac{1}{2} \text{Re} \left( \mathbf{E}^1 \times \mathbf{H}^1 \right)$  to be identified with the numerical Poynting vector, which is of course dimensionless.

With this definition of quantities, the complete RCWA can be calculated without entering physical constants like  $\epsilon_0$  or  $\mu_0$ . The true physical quantities can be derived after the calculation by multiplying with a constant physical term.

## Reference:

- [1] M.G. Moharam, Drew A. Pommet, Eric B. Grann, "Stable implementation of the rigorous coupled-wave analysis for surface-relief gratings: enhanced transmittance matrix approach", J. Opt. Soc. Am A, Vol. 12, No. 5, pp. 1077-1086, (1995)

## PUBLICATIONS

1. A. Junker, K.-H. Brenner, "Simulation and Analysis of SNOM Measurements using Rigorous Coupled-Wave Analysis", (Online-Zeitschrift der Deutschen Gesellschaft für angewandte Optik e. V.), ISSN: 1614-8436-urn:nbn:de:0287-2015-A019-6, 116. Jahrestagung, 26.-29. Mai 2015, Brno / Czech Republic, (2015)
2. A. Junker, K.-H. Brenner, "Structuring the incident and transmitted regions in rigorous coupled-wave analysis", 15<sup>th</sup> Workshop on Information Optics (WIO), IEEE, 978-1-5090-2163-5/16, 11.-15 Juli 2016, Barcelona, Spanien, (2016)
3. INVITED: K.-H. Brenner, M. Auer, "Verification of Near-field Calculations by Conservation Laws", 15<sup>th</sup> Workshop on Information Optics (WIO), IEEE, 978-1-5090-2163-5/16, 11.-15. Juli 2016, Barcelona, Spanien, (2016)
4. T. Stenau, K.-H. Brenner, "Light concentration efficiency of diffractive lenses with overlapping apertures", (Online-Zeitschrift der Deutschen Gesellschaft für angewandte Optik e. V.), ISSN: 1614-8436-urn:nbn:de:0287-2016-C017-5, 117. Jahrestagung, 17.-21. Mai 2016, Hannover, (2016)
5. T. Stenau, K.-H. Brenner, "Diffractive Lenses with Overlapping Aperture – A New Tool in Scanning Microscopy", Proceedings, Imaging and Applied Optics - Imaging Systems and Applications, OSA 2016, IT1F-1, ISBN: 978-1-9433580-15-6, <https://doi.org/10.1364/ISA.2016.IT1F.1>, 25.-28. Juli 2016, Heidelberg, (2016)

# IMPRINT

**Publisher:** Prof. Dr. Karl-Heinz Brenner  
Chair of Optoelectronics  
Institute of Computer Engineering (ZITI)  
Universität Heidelberg  
B6, 23-29, Bauteil C  
68131 Mannheim  
GERMANY

 +49 (0) 621 181 2700  
 +49 (0) 621 181 2695  
 <https://oe.ziti.uni-heidelberg.de/joomla/de/berichte.html>

**Layout:** K.-H. Brenner, S. Volk

**Type of publication:** Online

**Publication date:** 2017

For quotation of any of these contributions, please use:

**Reference:** Annual Report 2015-2016  
Chair of Optoelectronics,  
Universität Heidelberg  
ISSN 2197 - 4462